Food Hydrocolloids 94 (2019) 459–467

Contents lists available at ScienceDirect

Food Hydrocolloids

journal homepage: www.elsevier.com/locate/foodhyd

Combination of sodium alginate with tilapia fish gelatin for improved texture properties and nanostructure modification

Li Cheng Sow[a,b], Nicholas Zhen Yu Toh[c], Chong Wen Wong[c], Hongshun Yang[a,b,*]

[a] Food Science and Technology Programme, c/o Department of Chemistry, National University of Singapore, Singapore, 117543, Singapore
[b] National University of Singapore (Suzhou) Research Institute, 377 Lin Quan Street, Suzhou Industrial Park, Suzhou, Jiangsu, 215123, PR China
[c] NUS High School of Mathematics and Science, 20 Clementi Avenue 1, Singapore, 129957, Singapore

ARTICLE INFO

Keywords:
Fish gelatin
Polysaccharide
Nanostructure
CLSM
Atomic force microscopy
FTIR

ABSTRACT

Fish gelatin (FG) has been studied intensively as a potential replacement for mammalian gelatin; however, modification of the physicochemical properties of FG is often required to make them similar to those of mammalian gelatin. In the present study, sodium alginate (SA) was combined with tilapia FG to modify its properties to resemble those of mammalian gelatin. When the concentration of SA was increased from 0.05 to 0.4% (w/v) in a 6% (w/v) FG gel, the gel strength and hardness increased. However, at 0.60% (w/v) SA, the gel strength and hardness decreased. From 0.2 to greater than 0.4% SA, the gel changed from opaque to translucent. According to the zeta potential results, SA and FG associated via electrostatic interactions. The FG-SA complex coacervates, the SA fibrous network, and the FG-SA complex network were observed using atomic force microscopy. Based on the results, a schematic model was proposed, wherein at low SA concentrations ($\leq$0.2%), FG associates with SA, resulting in large, complex coacervates with a diameter up to 1064 nm. With increasing SA concentrations, formation of complex coacervates was promoted because of the excess of negatively charged SA, which led to complex networks. The complex network structure was coarser than that observed for SA or FG alone. Moreover, the schematic model was further validated at the microstructure level using confocal scanning laser microscopy and Fourier transform infrared spectroscopy. The nanostructure mismatch between FG-SA and pork gelatin resulted in a texture mismatch.

1. Introduction

Gelatin is hydrolysed from collagen using an acid or alkaline extraction process. Gelatin can associate from random coils into triple helices to form a thermoreversible physical gel (Doumèche, Picard, & Larreta-Garde, 2007; Feng, Bansal, & Yang, 2016). The triple helices contribute to gelatin's elastic properties, while the disordered peptide fragments contribute to the viscous properties (Ali, Kishimura, & Benjakul, 2018; Voron'ko, Derkach, & Izmailova, 2002). Fish gelatin (FG) has lower concentrations of imino acids (proline and hydroxyproline) compared with mammalian gelatin, which are critical for triple helix formation (Feng, Ng, Mikš-Krajnik, & Yang, 2017b; Razzak, Kim, & Chung, 2016). Thus, FG has suboptimal thermal and rheological properties compared with mammalian gelatin. To date, the extraction of FG from fish processing waste has contributed to sustainable food production (Feng, Fu, & Yang, 2017a), leading to a strong interest in using FG to replace mammalian gelatin.

One way to modify and improve the properties of FG is the addition of gelling agents, such as alginate. Alginate is a polysaccharide commonly obtained from brown seaweed, with a structure comprising repeating units of mannuronic acid (M) and guluronic acid (G) in the sequence of an M-M block, a G-G block, and an M-G block (Dong, Wang, & Du, 2006). The gelation mechanism of alginate relies on divalent salts (e.g. Ca^{2+}), which act as a salt bridge to crosslink the negatively charged alginate chain, forming an “egg-box” structure (Panouillé & Larreta-Garde, 2009). However, calcium-alginate gels are not thermoreversible.

A mixture of protein and polysaccharide could be miscible or phase separated. The phase separation could result from associative or segregative interactions. Mixed biopolymer gels can be categorised into three types, i.e., complex gels (coupled gels), mixed gels (interpenetrating gels), and filled gels (phase separated gels) (Zasypkin, Braudo, & Tolstoguzov, 1997), as a result of no-interaction (miscible), associative interaction, and segregative interaction, respectively.

Mixing of alginate and gelatin has been studied in the field of food, material science, and medicine. To form a complex coacervate between

* Corresponding author. Food Science and Technology Programme, c/o Department of Chemistry, National University of Singapore, Singapore, 117543, Singapore.
E-mail address: chmynghs@nus.edu.sg (H. Yang).

https://doi.org/10.1016/j.foodhyd.2019.03.041
Received 1 October 2018; Received in revised form 22 March 2019; Accepted 25 March 2019
Available online 28 March 2019
0268-005X/

Table 1
Effect of sodium alginate (SA) addition on the gel strength and texture profile analysis (TPA) of fish gelatin (FG).

Sample	Gel strength (g)	Hardness (N)	Springiness (%)	Cohesiveness	Chewiness (N)
PG	153.2 ± 3.4^{b}	16.9 ± 1.8^{a}	89.3 ± 1.3^{a}	0.947 ± 0.010^{a}	14.5 ± 1.8^{a}
FG	125.6 ± 2.9^{d}	13.3 ± 1.2^{c}	90.9 ± 2.8^{a}	0.914 ± 0.029^{b}	11.2 ± 1.3^{c}
FGA 0.05	129.8 ± 3.9^{d}	14.0 ± 0.9^{c}	91.2 ± 0.9^{a}	0.922 ± 0.010^{b}	11.8 ± 0.9^{bc}
FGA 0.2	151.4 ± 4.2^{b}	15.4 ± 1.0^{b}	91.3 ± 2.3^{a}	0.898 ± 0.011^{c}	12.5 ± 1.3^{b}
FGA 0.4	168.4 ± 4.2^{a}	15.9 ± 1.2^{b}	90.6 ± 2.2^{a}	0.858 ± 0.035^{d}	12.5 ± 1.3^{b}
FGA 0.6	135.9 ± 1.9^{c}	13.3 ± 0.6^{c}	90.9 ± 1.3^{a}	0.904 ± 0.023^{c}	11.0 ± 0.6^{c}

Within each column, means with different lowercase letters are significantly different ($P < 0.05$) among different groups.
PG refers to porcine gelatin; FGA 0.05, FGA 0.2, FGA 0.4, and FGA 0.6 refer to FG-SA mixed gels (6%, w/v) with 0.05%, 0.2%, 0.4%, and 0.6% of SA, respectively.

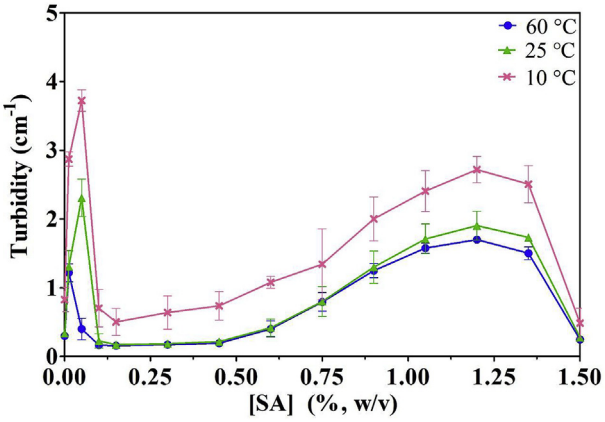

Fig. 1. The effect of sodium alginate (SA) addition on the turbidity of fish gelatin (FG) in a solution of 1.50% (w/v) total polymer concentration.

mammalian gelatin and alginate, low pH (3.5–3.8), crosslinking agents, and salts were applied (Dong et al., 2006; Doumèche et al., 2007; Fan et al., 2005; Panouillé et al., 2009; Saarai, Kasparkova, Sedlacek, & Saha, 2013; Saravanan & Rao, 2010; Shinde & Nagarsenker, 2009). In previous reports, the storage modulus or mechanical strength was improved in gelatin-alginate mixture. However, without crosslinking agents, various types of multicomponent gels were formed. Voron'ko et al. (2002) reported a filled gel comprising type B gelatin (1%, w/w) as the continuous matrix and SA (0.0001–0.15%, w/w) as the filler. Goudoulas and Germann (2017) found that type A pork gelatin (PG) and sodium alginate (SA) formed a homogenous binary gel (up to 5%, w/w) at a concentration ratio of 1:1. When cold water FG was mixed with SA at an 80:20 ratio at concentrations between 0.2 and 1% (w/v), a coupled network (complex gel) of FG and SA was observed (Razzak et al., 2016). As our understanding of the morphological and physicochemical properties of gelatin and natural food molecules increases (Dong, Padua, & Wang, 2013; Wang, Pan, McDonald, & Wang, 2017), it has become possible to develop a variety of ingredient replacers.

There have been no previous reports of mixing of tilapia FG (or other warm water FG), as a common food gelling agent, with SA. In addition, the ability of SA to modify the texture and nanostructure of FG, and the suitability of modified FG as mammalian gelatin replacer are unknown. Previously, we investigated the potential of two common food polysaccharides, low acyl gellan and κ-carrageenan, to mimic the textural properties of mammalian gelatin (Sow, Chong, Liao, & Yang, 2018a; Sow et al., 2017; Sow, Kong, & Yang, 2018b; Sow, Tan, & Yang, 2019). The formation of a segregative bi-continuous gellan and FG gel was proposed as a potential beef gelatin (BG) and PG replacer (Sow et al., 2017; 2018b). It would be interesting to investigate a mixture of alginate with gelatin, because alginate has a different gelling mechanism to low acyl gellan and κ-carrageenan, and might modify the structure of FG differently and more efficiently.

The objectives of this study were to investigate the ability of SA to modify the texture and structure of FG and to determine the

Table 2
Effective particle size (D_e), zeta potential, and pH of porcine gelatin (PG), fish gelatin (FG), and FG-SA (FGA) gels.

	D_e (nm)	Zeta potential (mV)	pH
PG	47.7 ± 23.7^{e}	8.6 ± 0.8^{a}	5.98 ± 0.12^{c}
FG	103.6 ± 22.5^{d}	2.2 ± 1.6^{b}	6.41 ± 0.10^{b}
FGA 0.05	796.1 ± 200.7^{b}	−3.7 ± 1.6^{c}	6.42 ± 0.14^{b}
FGA 0.2	1064.0 ± 134.9^{b}	−16.8 ± 2.3^{d}	6.51 ± 0.10^{b}
FGA 0.4	110.9 ± 32.4^{d}	−31.0 ± 5.0^{e}	6.60 ± 0.06^{b}
FGA 0.6	255.4 ± 78.6^{c}	−43.6 ± 0.9^{f}	6.67 ± 0.15^{b}
Alginate	1536.0 ± 152.0^{a}	−84.4 ± 9.7^{g}	6.92 ± 0.08^{a}

Within each column, means with different lowercase letters are significantly different ($P < 0.05$) among different groups.
The isoelectric points of PG and FG were pH 7.92 and 7.79, respectively (Sow et al., 2018b).

modification mechanism. Elucidating the nanostructure of an SA-FG system could increase our knowledge of the SA-FG interaction. Furthermore, studying the effect of SA on FG could help to screen appropriate modifications of FG by other ingredients using a similar experimental design.

2. Materials and methods

2.1. Materials

Tilapia (*Oreochromis aureus*) skin FG of 180 Bloom was purchased from Jiangxi Cosen Biology Co., Ltd (Yingtan, Jiangxi, China). PG was obtained from Qingdao Huachang Food Ingredients Co., Ltd (Qingdao, Shandong, China). SA (Protanal SF120RB) was obtained from FMC Health and Nutrition (Philadelphia, PA, USA), which contained 0.13% (w/w) calcium and 7.84% (w/w) sodium, based on inductive coupled plasma-optical emission spectroscopy (ICP-OES). The average molecular weight of FG, PG, and SA were 47,765; 29,617; and 91,198 Da, respectively (Bohidar, 1998; Martinsen, Skjåk-Bræk, Smidsrød, Zanetti, & Paoletti, 1991). All gelling agents were of food grade. ACS grade (> 99.9%) dimethyl sulphoxide (DMSO), HPLC grade rhodamine B (> 95%), and fluorescein isothiocyanate (FITC) (> 90%) were obtained from Sigma-Aldrich (St. Louis, MO, USA).

2.2. Gel preparation

All prepared gels had a total biopolymer concentration of 6% (w/v). Gelatin was soaked in deionised (DI) water for 2 h, and subsequently heated in a water bath at 65 °C for 10 min (Sow et al., 2018b). When the mixed gels were prepared, the DI water was divided into 1:1 vol for separate dissolution of the FG and SA solutions (0.05–0.6%, w/v) at 65 °C. The two solutions were then combined and stirred for 15 min to achieve a constant total biopolymer concentration of 6% (w/v). The hot solution was transferred into a cylindrical container with flat bottom (2.5 cm diameter, 3.1 cm height), and the gel was put in a small container and the container was put in an 8 ± 2 °C refrigerator (the temperature within the small container was 10 ± 1 °C) for 17 ± 1 h.

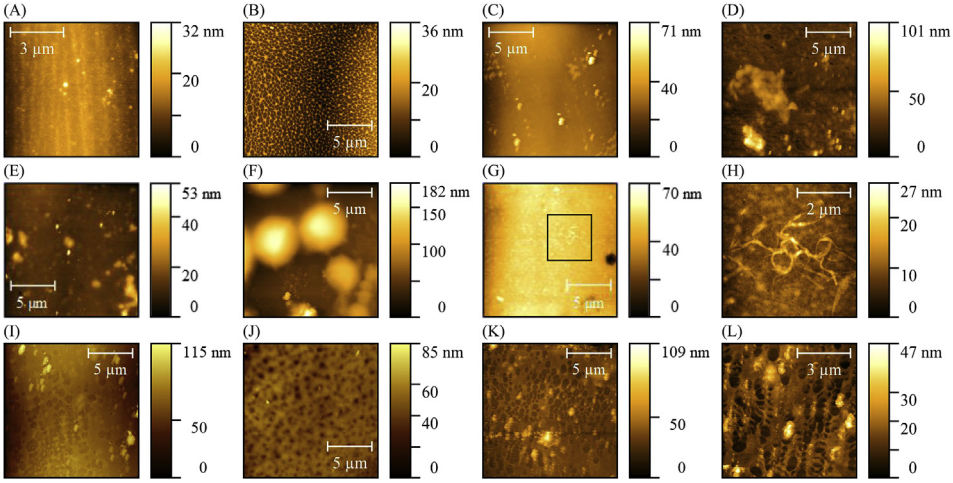

Fig. 2. Nanostructure of (A) porcine gelatin (PG); (B) sodium alginate (SA); (C) fish gelatin (FG), and FG-SA mixtures (FGA) of (D, E) FGA 0.05; (F, G, H) FGA 0.2; (I, J) FGA 0.4; (K, L) FGA 0.6. *FGA 0.05, FGA 0.2, FGA 0.4, and FGA 0.6 refer to FG-SA mixed gel (6%, w/v) with 0.05%, 0.2%, 0.4%, and 0.6% of SA, respectively.

Table 3
Summary of the nanostructures of porcine gelatin (PG), fish gelatin (FG), sodium alginate (SA), and FG-SA mixtures.

	PG	FG	FGA 0.05	FGA 0.2	FGA 0.4	FGA 0.6	SA
Spherical aggregates	+	+	+	+	+	+	–
Diameter (nm)	213.8 ± 87.0^{c}	362.9 ± 202.4^{b}	473.2 ± 332.8^{a}	372.4 ± 291.4^{b}	372.9 ± 229.6^{b}	349.3 ± 195.3^{b}	
Height (nm)	5.8 ± 7.1^{c}	13.2 ± 13.1^{b}	19.3 ± 19.2^{a}	16.6 ± 33.2^{a}	16.5 ± 16.4^{a}	17.5 ± 18.0^{a}	
Rods	+	+	–	–	+	–	+
Fibrils aggregates	–	–	–	+	–	–	+
Interconnecting network	–	–	–	–	+	+	+
Holes	–	+	+	+	+	+	–
Ring	–	+	–	–	+	+	–
Irregular aggregates	–	+	+	+	+	+	–
Amorphous region	–	–	–	+	+	+	+

The presence of a nanostructure is denoted as "+", while the absence of a nanostructure is denoted as "-".
Within each row, means with different lowercase letters are significantly different ($P < 0.05$) among different groups.

The samples containing SA concentrations (w/v) of 0.05%, 0.2%, 0.4%, and 0.6% in 6% (w/v) gel were labelled and referred to as FGA 0.05, FGA 0.2, FGA 0.4, and FGA 0.6, respectively.

2.3. Gel strength and texture profile analysis (TPA)

The gel was taken out of the cylindrical container and stored at 10 °C for subsequent gel strength and TPA analysis. A Texture Analyser (TA.XT2-i, Stable Micro System, Goldaming, Surrey, UK) was employed. The gel strength test was conducted using a cylindrical plunger (P/0.5 R) with a test speed of 0.5 mm/s and gel penetration distance of 4 mm. The TPA test was designed as a two-cycle compression test (40% compression distance) using a 47 mm flat plate (Sow et al., 2017; Yang et al., 2007).

2.4. Confocal laser scanning microscopy (CLSM)

The fluorescent markers FITC and rhodamine B were used to label SA and FG, respectively, (Razzak et al., 2016; Sow et al., 2018a). FITC and rhodamine B have different excitation and emission wavelengths of 490 and 525 nm and 540 and 625 nm, respectively. Separate dissolution of FG and SA (0.5%, w/v) was performed in DI water at 65 °C. FG was adjusted to pH 10.5 and SA to pH 8.5, followed by addition of the dye (2%, w/v, in DMSO) at a ratio of 25 μL of dye per 100 mL of FG or SA solution. Labelling was performed by mixing FG with rhodamine B and SA with FITC for 90 min at 65 °C, and then the pH was adjusted to the original pH. The rhodamine B-labelled FG and FITC-labelled SA were combined together according to the ratio of the mixed gels, as described in section 2.2. The sample was dried on a glass cover slide (1-mm thick) and stored under lightproof conditions at 4 °C. The microstructure was imaged using an Olympus FV1000 confocal scanning unit (Tokyo, Japan), equipped with argon ion and Helium-Neon (HeNe) lasers. The images were captured at 60× magnification with water immersion (PlanApo 60×/1.0 WLSM 0.17) and then processed using the Olympus Fluoview software (Olympus, Tokyo, Japan).

2.5. Atomic force microscopy (AFM)

The gels prepared in section 2.2 were melted and diluted to 0.1% (w/v) using DI water for nanostructure characterisation using table top (TT)-AFM (AFM workshop, Signal Hill, CA, USA). A probe (AppNano ACLA-10) of 160–225 kHz resonance frequency and 36–90 N/m force constant obtained from Applied NanoStructures (Mountain View, CA, USA) was used. The solution (20 μL) was deposited onto a freshly cleaved mica sheet (Sow & Yang, 2015; Zhou & Yang, 2019). The images were processed and analysed using Gwyddion software (http://gwyddion.net). To quantify the dimensions of spherical aggregates, line profile extraction was employed (Chen et al., 2018).

2.6. Turbidity

FG-SA mixtures were prepared at 1.5% (w/v) total biopolymer concentration, with the SA concentration in the mixture ranging from 0.0125% to 1.50% (w/v). For the measurements, the samples were incubated at 60, 25, and 10 °C for 1 h, respectively. Absorbance at 600 nm was recorded using a UV-1700 spectrophotometer (Shimadzu

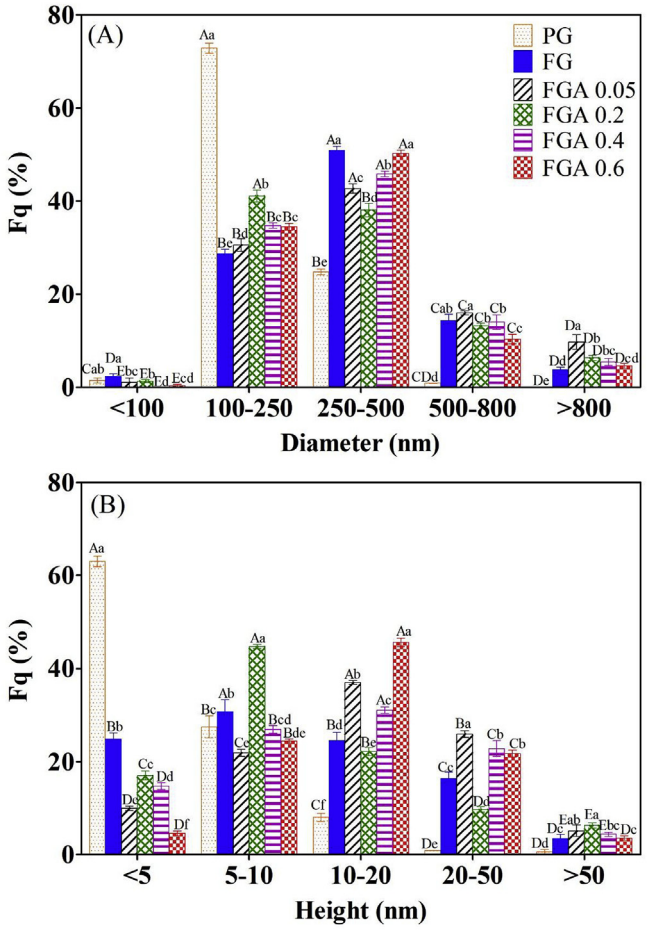

Fig. 3. Frequency distribution based on (A) diameter and (B) height of spherical aggregates identified from atomic force microscopy (AFM) images.*Within each dimension group, groups with different lowercase letters have significant statistical differences ($P < 0.05$). For the same sample, groups with different capital letters have significant statistical differences ($P < 0.05$) among different size ranges. *FGA 0.05, FGA 0.2, FGA 0.4, and FGA 0.6 refers to FG-SA mixed gel (6%, w/v) with 0.05%, 0.2%, 0.4%, 0.6% of SA, respectively. FG, fish gelatin; SA, sodium alginate; FGA, FG-SA mixture.

Corporation, Kyoto, Japan) and transformed into turbidity (τ, cm^{-1}) using the equation $\tau = -\frac{1}{L}\ln(\frac{I}{I_0})$, where I is the transmitted radiation intensity, I_0 is the intensity of incident radiation, and L is the light path length (Razzak et al., 2016).

2.7. Zeta potential and particle size

The samples prepared in section 2.2 were diluted to 0.01% (w/v) using hot (60 °C) DI water and stirred for 1 h at room temperature before measurement. A zeta potential and particle size analyser (NanoBrook Omni, Brookhaven Instruments, NY, USA) was used to study zeta potential with phase analysis light scattering (PALS) and the particle size was determined using dynamic light scattering (DLS). The Smoluchowski equation was applied to calculate the zeta potential (Sow et al., 2018b).

2.8. Fourier transform infrared (FTIR) spectroscopy

The lyophilised gel samples (3 mg) were ground and mixed with KBr (100 mg) before being pressed into a pellet. A Spectrum One FTIR spectrometer (PerkinElmer, Waltham, MA, USA) was used to collect the FTIR spectra. Scanning was performed from 4000 to 450 cm^{-1}, with a resolution of 4 cm^{-1}, and a scan number of 64. Baseline correction, smoothening, and Fourier self-deconvolution (1.5 Gamma, 50% width) of the spectra were carried out using the Spectrum software (version 5.0.1, PerkinElmer). The deconvoluted amide I band (1600–1700 cm^{-1}) was fitted to a Gaussian curve using Origin Pro 9 (OriginLab, Northampton, MA, USA). All spectra had a corrected $R^2 > 0.98$ (Sow & Yang, 2015) for the final fitting.

2.9. Statistical analysis

Three parallel experiments were carried out with at least triplicate samples within each analysis. For the AFM and CLSM experiments, dozens of parallel images were collected to ensure the statistical reliability of the feature dimension results. The results were reported in the format of the mean ± standard deviation (SD). One-way analysis of variance (ANOVA; $P < 0.05$) and Duncan's multiple range test were carried out to analyse the differences between samples using SPSS Statistics 20 software (IBM Corp., Armonk, NY,USA).

3. Results and discussion

3.1. Gel strength and TPA

The effect of SA on the gel strength and TPA of FG is shown in Table 1. The gel strength and hardness of FG increased when the concentration of SA increased from 0.05% to 0.4% (w/v) in the mixed gel, but decreased when SA reached 0.6% (w/v). In contrast, the cohesiveness of the FG-SA (FGA) gel decreased when SA was increased from 0.05 to 0.4% (w/v), while the cohesiveness increased slightly when SA was 0.6% (w/v). Interestingly, no significant changes in springiness were observed as a result of SA addition. In general, the FG-SA gel was not able to match the TPA profile of PG. As a comparison, the addition of 0.2% (w/v) κ-carrageenan into the same FG (5.98%, w/v) increased the gel strength, hardness, and chewiness to levels similar to those of PG (Sow et al., 2018b).

The sub-optimal performance of SA addition to improve FG's gel strength and TPA compared with low acyl gellan or κ-carrageenan addition might have been caused by different mechanisms. Bi-continuous network formation resulting from segregative FG-low acyl gellan interaction in the presence of Ca^{2+} was described as effective to improve the gel strength and TPA profile of FG (Sow et al., 2017, 2018b). Without the addition of Ca^{2+}, SA alone could not form a gel, thus the FG-SA gel was likely to be a complex or filled gel, where FG formed the supportive continuous matrix (Panouillé et al., 2009). Without free available Ca^{2+}, alginate could be confined to the gelatin continuous matrix, where it might interfere with the development of gelatin helices and network formation, thus decreasing the gel modulus (Panouillé et al., 2009). However, the results reported by Goudoulas et al. (2017) were promising, which showed that at the native pH, 5% gelatin with up to 2.5% SA resulted in an improved gel modulus. In addition, Voron'ko et al. (2002) reported a filled gel of SA-FG formed by 1% type B gelatin and 0.00013% SA, in which the continuous matrix was gelatin. The filled gel had improved rheological properties, including the yield point, viscosity, flow index, and consistency index (Voron'ko et al., 2002).

3.2. Turbidity, particle size, and zeta potential

Turbidity changes of the samples could be used as an indication of associative-complex coacervation caused by the electrostatic attraction of two oppositely charged biopolymers (Razzak et al., 2016; Zhao et al., 2019). Fig. 1 shows that the maximum turbidity occurred at 0.05% SA contained in a 1.5% (w/v) mixed gel; the ratio was the same as FGA 0.2 at 25 °C and 10 °C. Compared with the data in Table 2, which shows the effective particle size (D_e) and zeta potential, complex coacervates with a D_e of 1064 nm and a zeta potential of −16.8 mV were formed in FGA 0.2. Razzak et al. (2016) reported maximum complexation of cold

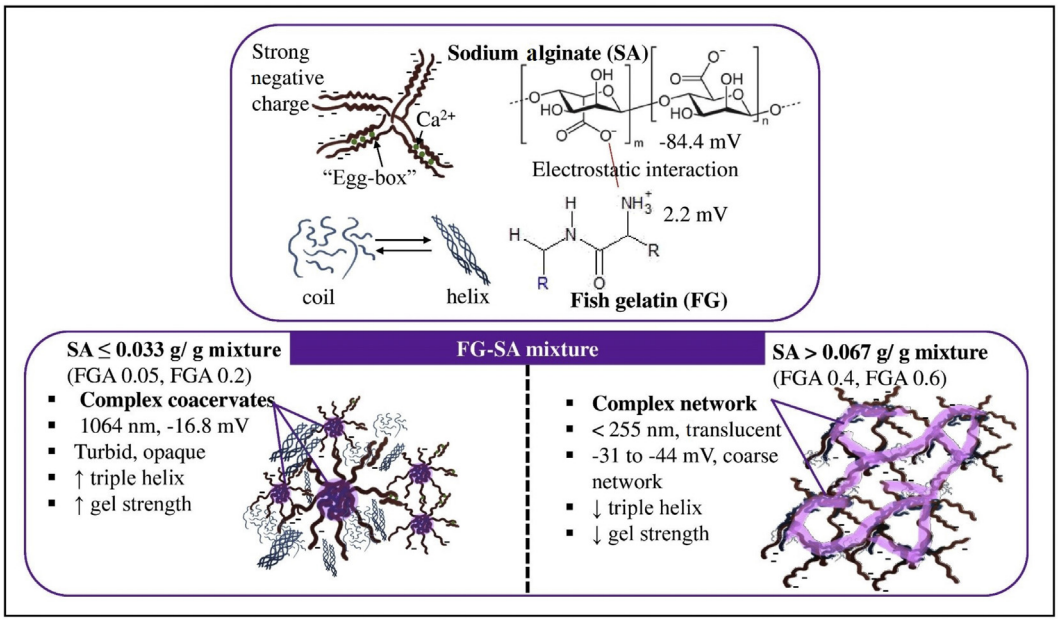

Fig. 4. The schematic mechanism of the structure and physicochemical property changes caused by the mixing of sodium alginate (SA) with fish gelatin (FG). *A small amount of Ca^{2+}(•) was present in the raw materials of SA; otherwise, no additional Ca^{2+} was added.

water FG and SA at an FG:SA (w/w) ratio of 80:20 and pH 3.7, in which the D_e was about 2000 nm. SA possessed a strong negative charge of −84.4 mV, while FG had a mild positive charge of 2.2 mV (Table 2). The electroneutrality of the complex formed was attributed to the effect of electrostatic-driven complex coacervation (Devi & Kakati, 2013). Although FGA 0.05 had a zeta potential close to neutral (−3.7 mV) compared with FGA 0.2 (−16.8 mV), the turbidity and particle size were greater in FGA 0.2, suggesting that the aggregation of complex-coacervates or other factors, such as a molecular ordering process, might also contribute to the high turbidity of FGA 0.2. The mild positive charge of FG might not be able to completely neutralise SA. Therefore, an excess of uncovered negatively charged patches could be expected in the FGA mixtures, resulting in an overall negative zeta potential (Xu, Luo, Liu, Zhang, & McClements, 2017).

The turbidity increased with decreasing temperature. At 60 °C, the maximum turbidity evolved at the low SA concentration of 0.0125% (w/v) per 1.50% (w/v) FG-SA mixture (the same as the ratio of SA:FG in FGA 0.05), which might indicate that the development of turbidity was also driven by reduced temperature. As the temperature decreased, the biopolymer underwent a molecular ordering process, in which the coil structure formed double and triple helices for SA and FG, respectively (Panouillé et al., 2009). The ordered structure could further aggregate, thus contributing to the increased turbidity (Razzak et al., 2016). The turbidity increased at high SA concentration from 0.60% to 1.50% (w/v; Fig. 1), which likely indicated more regions of interaction and structure modification, and should be investigated in future studies. Nevertheless, in the following sections concerning structural study, the SA concentration was limited to the concentration of FGA 0.6 (0.6% per 6% gel).

3.3. Nanostructure determination using AFM

Nanostructures of gelatin visualised by AFM could help to illustrate the nano-aggregation behaviour of gelatin, which is related to macro-scale properties (Liu & Wang, 2011). The nanostructures of the PG, SA, FG, and FGA mixtures are shown in Fig. 2, and the nanostructures identified are summarised in Table 3. PG and FG showed a majority of spherical and irregular aggregates (Fig. 2A, C), in which the mean diameter (d) and height (h) of spherical aggregates of FG (d = 362.9 nm, h = 13.2 nm) were larger than those of PG (d = 213.8 nm, h = 5.8 nm). This difference reflected their different molecular weights (Sow et al., 2018b) or state of aggregation. Table 2 shows that FG had zeta potential close to neutral charge. Without significant electrostatic repulsion, FG chains could associate into larger structures than PG. It was reported that the diameter of tilapia FG was between 201 and 472 nm (Sow et al., 2017, 2018b; Sow & Yang, 2015), while for PG it was about 197 nm (Sow et al., 2018b).

In the AFM imaging, SA showed a highly ordered interconnecting network (Fig. 2B), although the sample remained in a diluted liquid state (0.1%, w/v). When the water was evaporated off from the mica surface, SA chains could assemble and form a network, because of the Ca^{2+} (0.13%, w/w, dry basis) present in the raw material of SA. The current structure was comparable to the scanning electron microscope results presented by Saarai et al. (2013), who observed fibre-like structures and interconnected cross-linked SA networks in the presence of Ca^{2+}. Upon mixing, large and irregular aggregates were formed in FGA 0.05 (Fig. 2D and E), while for FGA 0.2, large spherical complex coacervates were found (Fig. 2F). In the region depleted of large complex coacervates, a high density of spherical and fibril aggregates was found (Fig. 2G and H). To provide a better view and resolution, a selected area (5 μm × 5 μm) of Fig. 2H (black square) was scanned and shown in Fig. 2G, where fibril aggregates emerged from the dense background of small spherical or irregular aggregates. The presence of fibril aggregates indicated there was an excess of SA in FGA 0.2, in addition to the SA that had associated and formed a complex coacervate with FG. This result correlated well with the overall negatively charged zeta potential of FGA 0.2 (Table 2). Therefore, the high turbidity of the FGA 0.2 gel was caused by both FG-SA complex coacervates and excess SA fibril aggregates.

An interconnecting network with voids (Fig. 2I, J, K, L), which showed increased hole size with increasing SA concentration, was identified in FGA 0.4 and FGA 0.6. The strands of the network appeared to be thicker than those of the SA network (Fig. 2J). Thus, it was not a mixed gel network (interpenetrating network), but could be a complex gel network formed by associated FG and SA. Zhao et al. (2019) also found that the electrostatic interaction between gelatin and SA-modified kudzu starch formed an interconnected network that had a different morphology from the pure components. The pore size of the continuous network was related to the crosslinking density of the gel (Liao, Zhang, & Chen, 2009); thus, the large hollow pores on the FGA

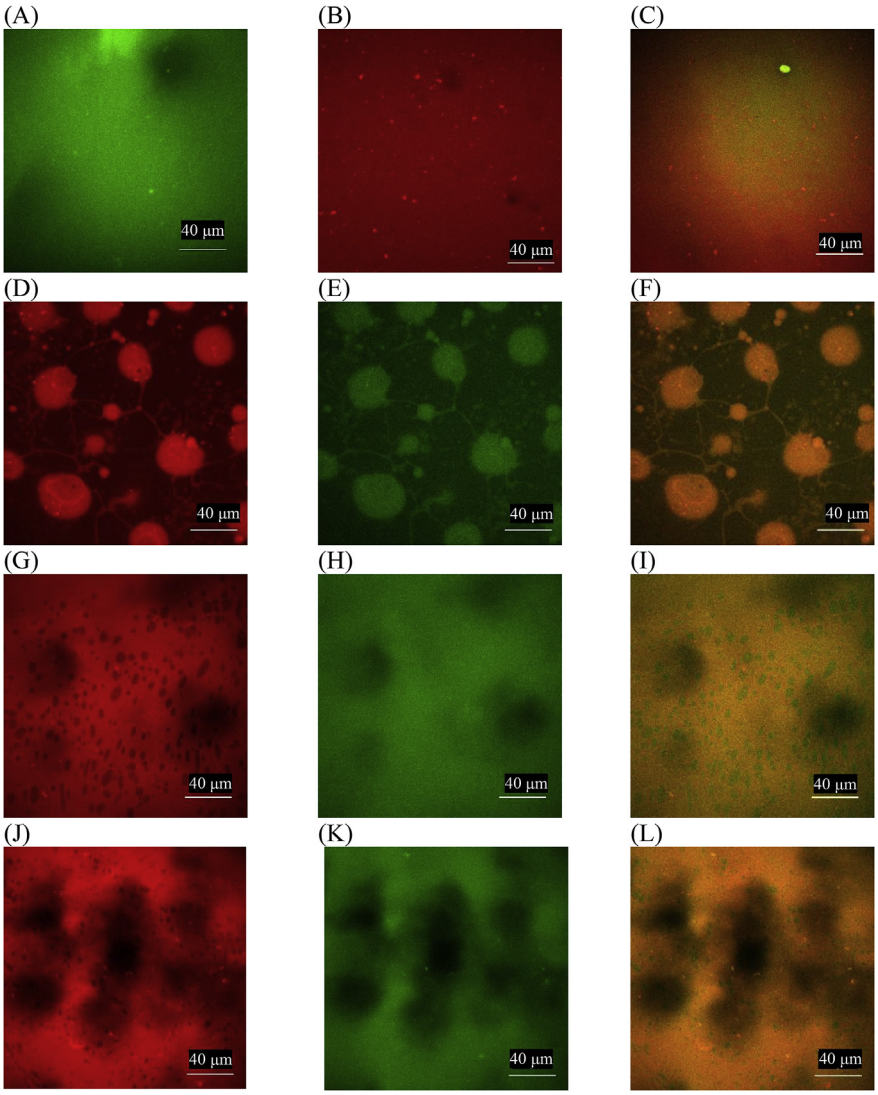

Fig. 5. Confocal laser scanning images of (A) sodium alginate (SA); (B) fish gelatin (FG); and FG-SA (FGA) mixture of (C) FGA 0.05; rhodamine channel (red) of (D) FGA 0.2, (G) FGA 0.4, (J) FGA 0.6; FITC channel (green) of (E) FGA 0.2, (H) FGA 0.4, (K) FGA 0.6; and the combined rhodamine and FITC channel of (F) FGA 0.2, (I) FGA 0.4 and (L) FGA 0.6. *FGA 0.05, FGA 0.2, FGA 0.4, and FGA 0.6 refer to FG-SA mixed gel (6%, w/v) with 0.05%, 0.2%, 0.4%, and 0.6% of SA, respectively. (For interpretation of the references to colour in this figure legend, the reader is referred to the Web version of this article.)

0.6 gel network might be related to a low crosslinking density, and hence the decreased gel strength (Table 1) (Sinthusamran, Benjakul, & Kishimura, 2014).

Quantification of the diameter and height of the spherical aggregates (Table 3) showed increased height of the aggregates in the FGA samples compared with those in FG alone. Only the diameter of spherical aggregates in FGA 0.05 was significantly greater than that of FG ($P < 0.05$). The increase in spherical diameter indicated the formation of complex coacervates, similar to the particle size results (Table 2). In previous studies (Sow et al., 2017, 2018b; Sow & Yang, 2015), a relationship between nanoaggregate dimensions and textural properties (e.g., TPA and gel strength) of FG was found, in systems comprising FG + NaCl and FG + low acyl gellan + Ca^{2+}. When the gel strength and hardness increased, a decrease in spherical aggregate size was observed (Sow et al., 2017, 2018b); however, when the gel strength and hardness decreased, large spherical aggregates were formed (Sow et al., 2015).

To account for the heterogeneous distribution of spherical aggregates, in addition to the average dimension of the spherical aggregates, the frequency distribution of various size groups of spherical aggregates was determined and compared. Sow et al. (2018b) reported that the frequency distribution in the group with diameters of 150–300 nm and heights of 0–5 nm was critical to differentiate PG from FG. For this critical dimension group, a similar frequency distribution compared with PG was reported for a FG-low acyl gellan formulation that successfully mimicked most of the physicochemical properties (gel strength, TPA, and melting temperature) of PG (Sow et al., 2018b). In Fig. 3, PG showed the highest frequency distribution in the 100–250 nm diameter range. The addition of SA increased the frequency distribution in the 100–250 nm diameter range, especially in FGA 0.2. The height distribution of PG was also significantly different from that of FG and FGA. For example, in PG, spherical aggregates with a height less than 5 nm were dominant. Similar average dimension of the nanospherical aggregates (Table 3) and the frequency distribution of the critical diameter and height group of PG were not observed in FGA samples, suggesting failure of the FGA mixtures to mimic the TPA properties of PG (Table 1).

3.4. Schematic model

To illustrate the modification of FG by SA, a schematic model was proposed (Fig. 4). The formation of complex coacervates was favoured

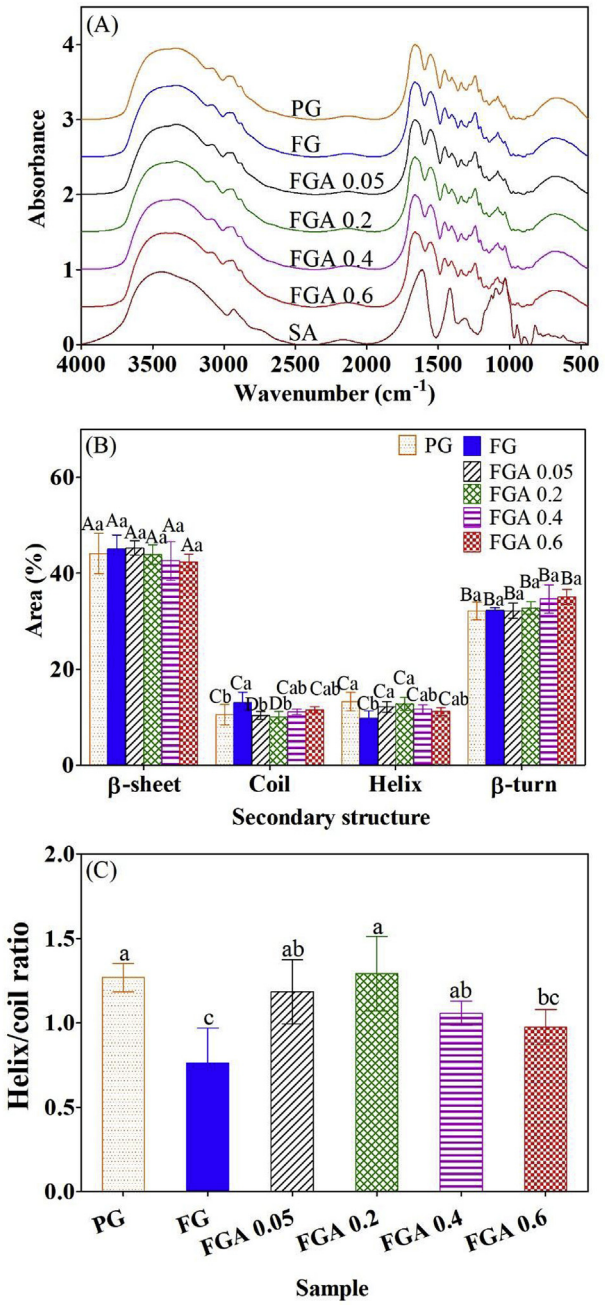

Fig. 6. Fourier transform infrared spectroscopy (FTIR) results for porcine gelatin (PG), fish gelatin (FG), sodium alginate (SA), and FG-SA (FGA) mixtures. (A) FTIR spectra; (B) secondary structure distribution; and (C) helix/coil ratio. *Within each secondary structure, samples with different lowercase letters have significant statistical differences ($P < 0.05$). For the same sample, groups with different capital letters have significant statistical differences ($P < 0.05$) among different size ranges. *FGA 0.05, FGA 0.2, FGA 0.4, and FGA 0.6 refer to FG-SA mixed gel (6%, w/v) with 0.05%, 0.2%, 0.4%, and 0.6% of SA, respectively.

when the SA concentration was equal to or below 0.033 g per 1 g in the mixture (0.2% in 6% (w/v) gel). The gel was opaque because of the presence of large particles, the emerged steric exclusion effect, the increased self-association of FG, and the enhanced gel strength of the network (Panouillé et al., 2009). With increased SA concentration in the FG gel (> 0.067 g SA per g mixture, equal to 0.4% SA in 6% gel, w/v), an excess of negatively charged SA chains resulted in stronger electrostatic repulsion, which reduced the formation of large size complex coacervates. Therefore, the FGA gel turned translucent. The complex gel network carried high negative charges; therefore, the crosslinking density was reduced by electrostatic repulsion, leading to a coarse network with decreased gel strength and hardness.

3.5. Model validation

3.5.1. CLSM

The microstructure of FG and FG-SA samples by CLSM is shown in Fig. 5, the results of which are comparable to the nanostructure (Fig. 2). Spherical complex coacervates, connected by fibril strands were found in FGA 0.2 (Fig. 5D, E, F). The spherical coacervates were formed by associative complexation between FG and SA, demonstrated by both individual channel images (Fig. 5D and E) of FGA 0.2 and the combined images (Fig. 5F). Previously, spherical complex coacervates were observed to form between FG and added gellan or κ-carrageenan (Sow et al., 2018b). Interestingly, this was the first time that complex coacervates of FG-SA connected by fibril strands were observed. Saravanan and Rao (2010) also reported small and uniform microspheres (< 10 μm), as alginate-gelatin complex coacervates, under scanning electron microscopy observation. In the current study, a coarse network with large holes was found in FGA 0.4 and FGA 0.6 (Fig. 5I, L). These morphologies showed that the complex network was formed by both FG and SA, which was supported by the individual rhodamine and FITC-labelled images (Fig. 5G, H, J, K), and the appearance of the yellow colour network in Fig. 5I, L. Interestingly, although the main backbone morphologies of FG and SA network were similar, the FG network contained voids (Fig. 2G, J). The depletion of FG might indicate a secondary segregative interaction in addition to the associative complexation and network formation. Previously, Fang, Li, Inoue, Lundin, and Appelqvist (2006) reported an associative-co-segregative structure in an FG and κ-carrageenan system, caused by the molecular ordering of κ-carrageenan that occurred with different kinetics to that of FG. Similarly, Razzak et al. (2016) reported that cold water FG and SA formed a complex network system, in which both biopolymers were associated together to form junction zones. Pang, Deeth, Yang, Prakash, and Bansal (2017) showed increased network density and decreased number of voids with increased FG concentration in acid milk gels. In the current study, the FG concentration was decreased in FGA 0.4 and FGA 0.6, which might have affected the network density.

3.5.2. FTIR

FTIR spectra were recorded to characterise the molecular interactions and secondary structure modification of FG (Fig. 6, Table 4). In general, the FTIR spectra of FG, PG, and FGA samples showed similar peaks and bands of amide A, amide I, amide II, and amide III, although with slight differences in the location of the peaks. The spectra of SA were different from those of FG at wavenumbers less than 1700 cm^{-1}. FGA 0.4 and FGA 0.6 showed significant modifications by SA, in which amide A was shifted to a high wavenumber (3376–3398 cm^{-1}) towards the O-H stretch peak of SA (3436 cm^{-1}). This shift indicated intermolecular hydrogen bond formation between OH groups in SA and NH groups of FG (Fan et al., 2005). There were additional peaks at 1123 cm^{-1} in FGA 0.4 and FGA 0.6 that were absent in FG, which might be the C-O stretching peaks of SA. The shifting of the peak towards a higher wavenumber close to that of SA (947 cm^{-1}) also occurred at the C-O stretch, at 942–944 cm^{-1} for FGA 0.4 and FGA 0.6, compared with FG at 938 cm^{-1}. Clearly, FGA 0.05 and FGA 0.2 behaved similarly to FG, while FGA 0.4 and FGA 0.6 had characteristics of both SA and FG.

There were differences in the wavenumber of amide I between FG and PG. To further analyse the differences, amide I (1600–1700 cm^{-1}) was deconvoluted and the component peaks were curve fitted and assigned to the various secondary structures, according to the wavenumber (Muyonga, Cole, & Duodu, 2004; Sow & Yang, 2015). Fig. 6B shows abundant and similar proportions of β-sheets and β-turn structures in all the samples, thus the critical difference in the secondary

Table 4
The assignments and indications of peaks identified from Fourier transform infrared spectroscopy (FTIR) spectra.

Region	Wavenumber (cm^{-1})							Assignment
	PG	FG	FGA0.05	FGA0.2	FGA0.4	FGA0.6	SA	
Amide A	3337 ± 3^{c}	3336 ± 5^{c}	3333 ± 4^{c}	3337 ± 4^{c}	3376 ± 48^{bc}	3398 ± 43^{b}	3436 ± 0^{a}	N-H stretch coupled with H-bond, O-H stretch
	2960 ± 0^{a}	2959 ± 1^{a}	2959 ± 0^{a}	2959 ± 0^{a}	2939 ± 1^{b}	2940 ± 8^{b}	2931 ± 0^{c}	CH_3 asymmetrical vibration
Amide I	1663 ± 1^{a}	1660 ± 0^{b}	1660 ± 1^{b}	1661 ± 2^{ab}	1660 ± 2^{b}	1660 ± 2^{b}	1620 ± 0^{c}	C=O stretch, COO- stretch (SA)
Amide II	1550 ± 1^{b}	1553 ± 2^{ab}	1554 ± 0^{ab}	1553 ± 1^{ab}	1553 ± 0^{ab}	1555 ± 4^{a}	1506 ± 1^{c}	NH bend coupled with CN stretch
	1453 ± 0^{ab}	1453 ± 0^{ab}	1453 ± 0^{ab}	1453 ± 0^{ab}	1454 ± 0^{a}	1453 ± 0^{b}		CH_2 deformation
	1404 ± 0^{cd}	1404 ± 0^{d}	1404 ± 0^{d}	1404 ± 0^{cd}	1405 ± 1^{bc}	1406 ± 1^{b}	1416 ± 0^{a}	$COO-$ symmetrical stretch
	1338 ± 1^{a}	1337 ± 1^{a}	1337 ± 0^{a}	1336 ± 1^{a}	1338 ± 0^{a}	1338 ± 2^{a}	1316 ± 0^{b}	CH_2 wag of proline & glycine; CO stretching in $COO-$
Amide III	1241 ± 1^{a}	1240 ± 0^{a}	1240 ± 0^{a}	1240 ± 0^{a}	1240 ± 0^{a}	1241 ± 1^{a}		NH stretch coupled with CN stretch
	1163 ± 0^{a}	1163 ± 0^{a}	1163 ± 0^{a}	1162 ± 0^{a}	1162 ± 0^{a}	1163 ± 1^{a}		C–O stretching
					1123 ± 0	1123 ± 1	1126 ± 0	C–O stretching
Fingerprint	1082 ± 0^{b}	1082 ± 0^{b}	1082 ± 0^{b}	1082 ± 0^{b}	1082 ± 0^{b}	1083 ± 1^{a}	1096 ± 0	C-O stretch
	1033 ± 0^{a}	1032 ± 0^{a}	1033 ± 0^{a}	1032 ± 0^{a}	1032 ± 0^{b}	1032 ± 0^{b}	1030 ± 0^{c}	C-O stretch
	937 ± 1^{d}	938 ± 0^{d}	939 ± 1^{d}	940 ± 2^{c}	942 ± 1^{c}	944 ± 1^{b}	947 ± 0^{a}	C-O stretch, uronic acids C-O stretch (SA)
	875 ± 1^{ab}	874 ± 3^{b}	875 ± 1^{ab}	875 ± 2^{ab}	875 ± 1^{ab}	876 ± 1^{a}		C-H deformation of mannuronic acid (SA)
	845 ± 5^{a}	845 ± 2^{a}	849 ± 4^{a}	848 ± 3^{a}	850 ± 3^{a}	850 ± 1^{a}	822 ± 0^{b}	Mannuronic acid residue (SA)
	672 ± 6^{a}	686 ± 18^{a}	682 ± 21^{a}	683 ± 12^{a}	682 ± 10^{a}	691 ± 15^{a}	784 ± 0	Guluronic acid residue (SA)

Within each row, means with different lowercase letters are significantly different ($P < 0.05$) among different groups.
The assignment of peaks was performed according to reports from Papageorgiou et al. (2010) and Sow and Yang (2015).

structure was the proportion of helices and coils, or the helix/coil ratio (Fig. 6C). The proportions of helices and coils in the PG and FGA gels were similar, while FG had fewer helices and more coils than PG. The helix/coil ratio (Fig. 6C), which is known to be related to the triple helix content (Sow et al., 2017), increased when SA was added, with the maximum triple helix content found in FGA 0.2. This indicated that the increased gel strength of the FGA gel (up to FGA 0.4) could be caused by a higher triple helix content. In FGA 0.6, the decrease in the triple helix content led to decreased gel strength at high concentrations of SA. The formation of triple helices relied on the aggregation of the FG chain in an ordered manner, in which the steric exclusion force could repel and push the FG chains together, therefore increasing the opportunity of FG chains to associate and increasing the triple helix content (Panouillé et al., 2009; Sow et al., 2017). In FGA 0.6, FG associated with SA, resulting in a complex gel that was different from the network of FG or SA. The formation of the interpolymeric junction zone of FG-SA might inhibit the formation of triple helices, which serve as junction zones in FG gels.

4. Conclusion

FG and SA could associate with each other under native pH conditions (pH 6.67–6.41) through electrostatic interactions. At low concentrations of SA (≤0.2% (w/v) SA in 6% (w/v) gel) FG-SA complex coacervates formed with a maximum size of 1064 ± 135 nm. The formation of complex coacervates, and the increase in the triple helix content, contributed to the increase in turbidity, gel strength, and hardness of the gel. At high SA concentrations (≥0.4% (w/v) in 6% (w/v) gel) a complex gel was formed, whose coarse structure led to decreased gel strength and hardness. None of the FGA samples exhibited similar critical nanoaggregate properties to PG, either in terms of the mean spherical aggregate size or the aggregate distribution. Therefore, matching of the textural profile properties of FGA with PG was not successful, which contrasted with the results of combining FG with other polysaccharides (e.g., low acyl gellan).

Acknowledgements

Projects 31471605 and 31200801 supported by NSFC; Singapore Ministry of Education Academic Research Fund Tier 1 (R-143-000-A40-114), and industry projects from Fujian Putian Sea-100 Food Co., Ltd. (R-143-000-633-597) and Fujian Changle Juquan Food Co., Ltd. (R-143-000-A73-597) contributed to this research.

References

Ali, A. M. M., Kishimura, H., & Benjakul, S. (2018). Physicochemical and molecular properties of gelatin from skin of golden carp (*Probarbus Jullieni*) as influenced by acid pretreatment and prior-ultrasonication. *Food Hydrocolloids, 82*, 164–172.
Bohidar, H. B. (1998). Hydrodynamic properties of gelatin in dilute solutions. *International Journal Of Biological Macromolecules, 23*, 1–6.
Chen, L., Zhou, Y., He, Z., Liu, Q., Lai, S., & Yang, H. (2018). Effect of exogenous ATP on the postharvest properties and pectin degradation of mung bean sprouts (*Vigna radiata*). *Food Chemistry, 251*, 9–17.
Devi, N., & Kakati, D. K. (2013). Smart porous microparticles based on gelatin/sodium alginate polyelectrolyte complex. *Journal of Food Engineering, 117*, 193–204.
Dong, F., Padua, G., & Wang, Y. (2013). Controlled formation of hydrophobic surfaces by self-assembly of an amphiphilic natural protein from aqueous solutions. *Soft Matter, 9*, 5933–5941.
Dong, Z., Wang, Q., & Du, Y. (2006). Alginate/gelatin blend films and their properties for drug controlled release. *Journal of Membrane Science, 280*, 37–44.
Doumèche, B., Picard, J., & Larreta-Garde, V. (2007). Enzyme-catalyzed phase transition of alginate gels and gelatin−alginate interpenetrated networks. *Biomacromolecules, 8*, 3613–3618.
Fan, L., Du, Y., Huang, R., Wang, Q., Wang, X., & Zhang, L. (2005). Preparation and characterization of alginate/gelatin blend fibers. *Journal of Applied Polymer Science, 96*, 1625–1629.
Fang, Y., Li, L., Inoue, C., Lundin, L., & Appelqvist, I. (2006). Associative and segregative phase separations of gelatin/κ-carrageenan aqueous mixtures. *Langmuir, 22*, 9532–9537.
Feng, X., Bansal, N., & Yang, H. (2016). Fish gelatin combined with chitosan coating inhibits myofibril degradation of golden pomfret (Trachinotus blochii) fillet during cold storage. *Food Chemistry, 200*, 283–292.
Feng, X., Fu, C., & Yang, H. (2017a). Gelatin addition improves the nutrient retention, texture and mass transfer of fish balls without altering their nanostructure during boiling. *Lebensmittel-Wissenschaft und -Technologie- Food Science and Technology, 77*, 142–151.
Feng, X., Ng, V. K., Mikš-Krajnik, M., & Yang, H. (2017b). Effects of fish gelatin and tea polyphenol coating on the spoilage and degradation of myofibril in fish fillet during cold storage. *Food and Bioprocess Technology, 10*, 89–102.
Goudoulas, T. B., & Germann, N. (2017). Phase transition kinetics and rheology of gelatin-alginate mixtures. *Food Hydrocolloids, 66*, 49–60.
Liao, H., Zhang, H., & Chen, W. (2009). Differential physical, rheological, and biological properties of rapid in situ gelable hydrogels composed of oxidized alginate and gelatin derived from marine or porcine sources. *Journal of Materials Science: Materials in Medicine, 20*, 1263–1271.
Liu, S., & Wang, Y. (2011). Chapter 6 - a review of the application of atomic force microscopy (AFM) in food science and technology. In L. T. Steve (Ed.). *Advances in food and nutrition research* (pp. 201–240). Academic Press.
Martinsen, A., Skjåk-Bræk, G., Smidsrød, O., Zanetti, F., & Paoletti, S. (1991). Comparison of different methods for determination of molecular weight and molecular weight distribution of alginates. *Carbohydrate Polymers, 15*, 171–193.
Muyonga, J. H., Cole, C. G. B., & Duodu, K. G. (2004). Fourier transform infrared (FTIR) spectroscopic study of acid soluble collagen and gelatin from skins and bones of young and adult Nile perch (*Lates niloticus*). *Food Chemistry, 86*, 325–332.
Pang, Z., Deeth, H., Yang, H., Prakash, S., & Bansal, N. (2017). Evaluation of tilapia skin gelatin as a mammalian gelatin replacer in acid milk gels and low-fat stirred yogurt. *Journal of Dairy Science, 100*, 3436–3447.
Panouillé, M., & Larreta-Garde, V. (2009). Gelation behaviour of gelatin and alginate mixtures. *Food Hydrocolloids, 23*, 1074–1080.

Papageorgiou, S. K., Kouvelos, E. P., Favvas, E. P., Sapalidis, A. A., Romanos, G. E., & Katsaros, F. K. (2010). Metal–carboxylate interactions in metal–alginate complexes studied with FTIR spectroscopy. *Carbohydrate Research, 345*, 469–473.

Razzak, M. A., Kim, M., & Chung, D. (2016). Elucidation of aqueous interactions between fish gelatin and sodium alginate. *Carbohydrate Polymers, 148*, 181–188.

Saarai, A., Kasparkova, V., Sedlacek, T., & Saha, P. (2013). On the development and characterisation of crosslinked sodium alginate/gelatine hydrogels. *Journal of the Mechanical Behavior of Biomedical Materials, 18*, 152–166.

Saravanan, M., & Rao, K. P. (2010). Pectin–gelatin and alginate–gelatin complex coacervation for controlled drug delivery: Influence of anionic polysaccharides and drugs being encapsulated on physicochemical properties of microcapsules. *Carbohydrate Polymers, 80*, 808–816.

Shinde, U. A., & Nagarsenker, M. S. (2009). Characterization of gelatin-sodium alginate complex coacervation system. *Indian Journal of Pharmaceutical Sciences, 71*, 313–317.

Sinthusamran, S., Benjakul, S., & Kishimura, H. (2014). Characteristics and gel properties of gelatin from skin of seabass (*Lates calcarifer)* as influenced by extraction conditions. *Food Chemistry, 152*, 276–284.

Sow, L. C., Chong, J. M. N., Liao, Q. X., & Yang, H. (2018a). Effects of κ-carrageenan on the structure and rheological properties of fish gelatin. *Journal of Food Engineering, 239*, 92–103.

Sow, L. C., Kong, K., & Yang, H. (2018b). Structural modification of fish gelatin by the addition of gellan, κ-carrageenan, and salts mimics the critical physicochemical properties of pork gelatin. *Journal of Food Science, 83*, 1280–1291.

Sow, L. C., Peh, Y. R., Pekerti, B. N., Fu, C., Bansal, N., & Yang, H. (2017). Nanostructural analysis and textural modification of tilapia fish gelatin affected by gellan and calcium chloride addition. *Lebensmittel-Wissenschaft und -Technologie- Food Science and Technology, 85*, 137–145.

Sow, L. C., Tan, S. J., & Yang, H. (2019). Rheological properties and structure modification in liquid and gel of tilapia skin gelatin by addition of low acyl gellan. *Food Hydrocolloids, 90*, 9–18.

Sow, L. C., & Yang, H. (2015). Effects of salt and sugar addition on the physicochemical properties and nanostructure of fish gelatin. *Food Hydrocolloids, 45*, 72–82.

Voron'ko, N. G., Derkach, S. R., & Izmailova, V. N. (2002). Rheological properties of gels of gelatin with sodium alginate. *Russian Journal of Applied Chemistry, 75*, 790–794.

Wang, B., Pan, P., McDonald, T. P., & Wang, Y. (2017). Development of a capacitance sensing system for monitoring moisture content of spray dried gelatin powders. *Journal of Food Engineering, 195*, 247–254.

Xu, X., Luo, L., Liu, C., Zhang, Z., & McClements, D. J. (2017). Influence of electrostatic interactions on behavior of mixed rice glutelin and alginate systems: pH and ionic strength effects. *Food Hydrocolloids, 63*, 301–308.

Yang, H., Wang, Y., Jiang, M., Oh, J., Herring, J., & Zhou, P. (2007). 2-step optimization of the extraction and subsequent physical properties of channel catfish (*Ictalurus punctatus*) skin gelatin. *Journal of Food Science, 72*, C188–C195.

Zasypkin, D. V., Braudo, E. E., & Tolstoguzov, V. B. (1997). Multicomponent biopolymer gels. *Food Hydrocolloids, 11*, 159–170.

Zhao, Y., Khalid, N., Shu, G., Neves, M. A., Kobayashi, I., & Nakajima, M. (2019). Complex coacervates from gelatin and octenyl succinic anhydride modified kudzu starch: Insights of formulation and characterization. *Food Hydrocolloids, 86*, 70–77.

Zhou, Y., & Yang, H. (2019). Effects of calcium ion on gel properties and gelation of tilapia (*Oreochromis niloticus*) protein isolates processed with pH shift method. *Food Chemistry, 277*, 327–335.